Arch Appl Mech (2014) 84:343–353
DOI 10.1007/s00419-013-0803-0

ORIGINAL

Chiping Jiang · Hui Chai · Peng Yan · Fan Song

The interaction of a screw dislocation with a circular inhomogeneity near the free surface

Received: 25 June 2013 / Accepted: 15 November 2013 / Published online: 3 December 2013

Abstract The interaction of a screw dislocation with a circular inhomogeneity near the free surface is discussed in this paper. By using the complex potential and conformal mapping technique, an explicit series solution is obtained. Then, the solution is cast into a new expression to separate the interaction effects between the dislocation, inhomogeneity, and free surface. The new expression is not only convenient to reveal the coupling interaction effects, but also helpful to improve the convergence of the solution. As an application of the new expression, a simple approximate formula is presented with high accuracy. Finally, the full-field interaction energy and image force are evaluated and studied graphically. It is found that when the screw dislocation, inhomogeneity, and free surface are close to each other, their interaction effects strongly and intricately couple in the near field. In the case of a soft inhomogeneity or a hole, there is an unstable equilibrium point of the screw dislocation between the inhomogeneity and free surface, whereas in the case of a hard or rigid inhomogeneity, there is an unstable equilibrium point on the opposite side of the inhomogeneity.

Keywords Dislocations · Free surface · Complex potential method · Coupling interaction · Simple approximate solution

1 Introduction

The interaction of a dislocation with inhomogeneities is a very important topic in the study of strengthening and deformation mechanism of many heterogeneous materials. It is because that such an interaction induces an image forces acting on the dislocation, and consequently induces a motion of the dislocation. From Head's work [1], many researches have been performed. It is revealed that the interaction energy and image force acting on the dislocation are significantly influenced by the shape of inhomogeneities [1–6], the nature of inhomogeneity/matrix interfaces [7–10], and the size of inhomogeneities [11–13].

In 1953, Head [1] first derived the image force on a dislocation near a straight interface between two dissimilar materials. He found that the dislocation was either repealed or attracted by the interface, depending on the combination of material constants. The interaction of the dislocation with various shapes of inhomogeneities

C. Jiang (✉) · H. Chai · P. Yan
School of Aeronautic Science and Engineering, Beihang University,
Beijing 100191, China
E-mail: jiangchiping@buaa.edu.cn

C. Jiang · F. Song
State Key Laboratory of Nonlinear Mechanics (LNM), Institute of Mechanics,
Chinese Academy of Sciences, Beijing 100190, China

had been well studied since then. Smith [2] analyzed the cases of inhomogeneities with circular or elliptic sections and derived the series solutions. By using the Eshelby equivalent inclusion method, Li and Shi [3] studied more general cases of inhomogeneities with arbitrary shape, and obtained a set of simple approximate formulae with satisfactory accuracy to determine the image force. As an extension to the piezoelectric issue, Shen et al. [4] investigated the interaction between a screw dislocation and a piezoelectric fiber composite with a semi-infinite wedge crack. Zeng et al. [5] dealt with the interaction between piezoelectric screw dislocations and two asymmetrical interfacial cracks emanating from an elliptic hole under combined mechanical and electric load at infinity. Zhang et al. [6] presented a numerical solution of interaction between cracks and a circular inclusion in a finite plate, in which distributed dislocations were used to model the cracks and boundaries.

Due to the presence of materials such as fiber coating or transitional layers between inhomogeneities and the matrix, it is more reasonable in many cases to consider an interface as an interphase layer with finite thickness. Many works have been done to study the interaction between a dislocation and inhomogeneities with different nature of interfaces. Xiao and Chen [7] considered a circular coated fiber and obtained a closed-form solution for the stress. Jiang et al. [8] considered the problem of the interaction of a screw dislocation with an interphase layer between a circular inclusion and a matrix and obtained explicit series solutions by combining the sectionally holomorphic function, Cauchy integral and Laurent series expansion techniques. Honein et al. [9] studied a multi-layered interphase between a circularly cylindrical inclusion and a matrix, where the layers were coaxial cylinders of annular cross-sections with arbitrary radii and different shear moduli, and the number of layers may also be arbitrary. Sudak [10] considered a circular inhomogeneity with homogeneous imperfect interface undergoing uniform eigenstrains.

In another important case, though there is no such a coating layer, since the equilibrium lattice spacing in the interface is different from that in the bulk, the interface stress effect must be considered when the inhomogeneity is small to nano-size. By introducing the interface stress effects of the nano-inhomogeneity with the Gurtin–Murdoch model, Fang and Liu [11] investigated the interaction of a screw dislocation with a circular nano-inhomogeneity, and they found that the normalized image force depended on the inhomogeneity size. The interface effect becomes negligible when the radius of the inhomogeneity is relatively large. Luo and Xiao [12] obtained the solution of semi-analytical nature for a screw dislocation interacting with an elliptical nano-inhomogeneity. Ahmadzadeh-Bakhshayesh et al. [13] dealt with the surface/interface effects on elastic behavior of a screw dislocation in an eccentric core-shell nanowire.

Actually, free surface is another important factor in some of the interaction issues of dislocations. Experimental investigations revealed interesting interaction phenomena of dislocations with free surfaces [14–17]. The theoretical solution of the interaction of a dislocation with the free surface was firstly given by Head [1]. When a dislocation approaches an inhomogeneity near the free surface, an intricate coupling interaction effect occurs. The solution of the problem cannot be obtained by a linear superposition of Head's result and the solution of a dislocation near an inhomogeneity in an infinite medium. The purpose of this paper is to study such an interesting coupling phenomenon.

This paper is organized as follows. Section 2 formulates the basic equations. Section 3 provides an exact series solution of the complex potential by using the conformal mapping technique. Section 4 shows that the present solution can degenerate into many existing solutions, and this fact suggests a new expression of the present solution, where various interaction effects are separated. Section 5 derives the interaction energy and image force. It is found that the new expression not only is convenient to investigation, but also converges more rapidly. A simple approximate formula with high accuracy is presented. The exact full-field distributions of the interaction energy and image force are evaluated and shown graphically by two illustrative examples. In Sect. 6, several conclusions are drawn.

2 Problem description and basic equations

Consider a screw dislocation with the Burgers vector $\boldsymbol{b}$ near a circular isotropic inhomogeneity and the free surface in a semi-infinite isotropic medium as shown in Fig. 1a, where the radius of the inhomogeneity is R_1, the origin of a Cartesian coordinate system lies at the center of the inhomogeneity and the x-axis is perpendicular to the free surface. Let h be the distance between the inhomogeneity and the free surface; z_0 denotes the location of the screw dislocation; D_1, D_2 and D_3 denote the regions occupied by the inhomogeneity, the semi-infinite medium, and the outside of the medium, respectively; $\mathbf{\Gamma}_1$ and $\mathbf{\Gamma}_2$ denote the inhomogeneity/medium interface and the free surface of the medium, respectively.

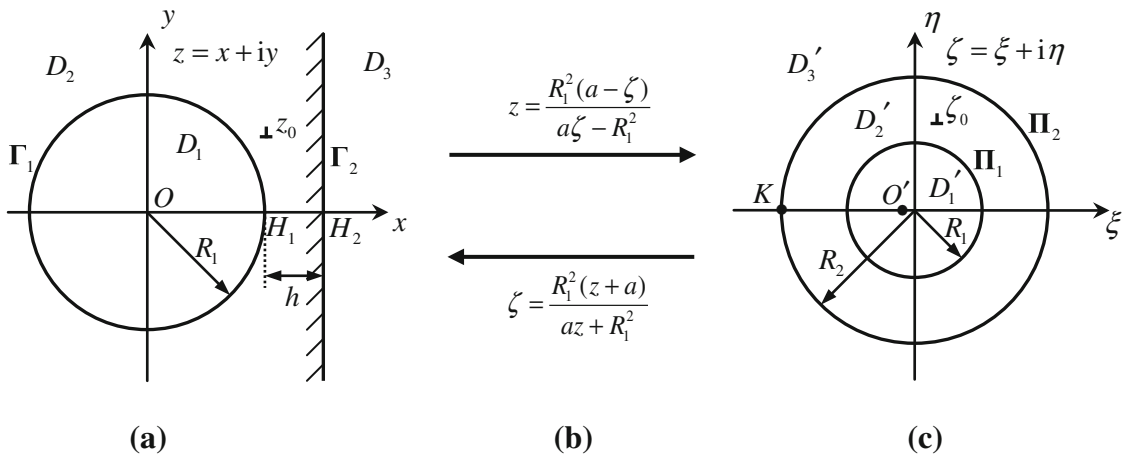

Fig. 1 **a** A screw dislocation near a circular isotropic inhomogeneity and the free surface. **b** Conformal mapping. **c** Mapping region

In anti-plane strain state, the displacement w, the shear stress components τ_{xz} and τ_{yz}, and the resultant force T along any arc AB in the material can be expressed in terms of a single analytical function (complex potential) $f(z)$ of the complex variable $z = x + \mathrm{i}y$ as follows [18]

$$w = \frac{1}{2\mu}\left[f(z) + \overline{f(z)}\right], \tag{1}$$

$$\tau_{xz} - \mathrm{i}\tau_{yz} = f'(z) \tag{2}$$

$$T = \int_A^B \left(\tau_{xz}\mathrm{d}y - \tau_{yz}\mathrm{d}x\right) = \frac{\mathrm{i}}{2}\left[\overline{f(z)} - f(z)\right]_A^B, \tag{3}$$

where μ is the shear modulus of the material, the overbar represents the complex conjugate, the superscript prime denotes the differentiation with respect to the argument, $[\cdot]_A^B$ signifies the change in the bracketed function in going from the point A to the point B along any arc AB. $f(z)$ is holomorphic in the region occupied by the elastic medium, but poles at the screw dislocation points. The assumption of a perfect bonding between dissimilar materials implies the continuity conditions of stresses and displacements. The stress continuity may also be integrated to become resultant force continuity conditions. These conditions can be expressed as

$$w_1 = w_2,\ T_1 = T_2 \text{ on } \boldsymbol{\Gamma_1}, \tag{4}$$

$$T_2 = 0 \text{ on } \boldsymbol{\Gamma_2}, \tag{5}$$

where and hereafter the subscripts 1 and 2 refer to the inhomogeneity and the semi-infinite medium, respectively.

By analyzing the singularities of the complex functions, it is seen that $f_1(z)$ in D_1 is holomorphic and $f_2(z)$ in D_2 can be expressed as

$$f_2(z) = \frac{\mu_2 b}{2\pi\mathrm{i}}\ln(z - z_0) + f_{20}(z) \text{ in } D_2 \tag{6}$$

where $f_{20}(z)$ is the holomorphic part of $f_2(z)$, b is the module of the Burgers vector $\boldsymbol{b}$.

3 Solutions of the complex potential

3.1 Conformal mapping

In order to solve the above problem, the conformal mapping is introduced as

$$z = m(\zeta) = \frac{R_1^2(a - \zeta)}{a\zeta - R_1^2} \tag{7}$$

where $\zeta = \xi + \mathrm{i}\eta$, $a = -(R_1+h)+\sqrt{(R_1+h)^2 - R_1^2}$, $R_2 = (R_1+h)+\sqrt{(R_1+h)^2 - R_1^2}$ and $aR_2 = -R_1^2$. The regions D_1, D_2 and D_3 in Fig. 1a are, respectively, mapped onto the regions $D_1'(|\zeta| < R_1)$, $D_2'(R_1 < |\zeta| < R_2)$ and $D_3'(|\zeta| > R_2)$ in Fig. 1c. $\mathbf{\Gamma}_1$ and $\mathbf{\Gamma}_2$ are mapped onto $\mathbf{\Pi}_1$ and $\mathbf{\Pi}_2$, respectively. The coordinate origin O, the infinity, and the point z_0 are, respectively, mapped onto the points $O'(\zeta = a)$, $K(\zeta = -R_2)$ and ζ_0. It is noted that the radii of both $\mathbf{\Gamma}_1$ and $\mathbf{\Pi}_1$ are R_1.

In the ζ-plane, Eqs. (1), (2) and (3) become

$$w = \frac{1}{2\mu}\left[\varphi(\zeta) + \overline{\varphi(\zeta)}\right], \tag{8}$$

$$\tau_{xz} - \mathrm{i}\tau_{yz} = \frac{\varphi'(\zeta)}{m'(\zeta)}, \tag{9}$$

$$T = \frac{\mathrm{i}}{2}\left[\overline{\varphi(\zeta)} - \varphi(\zeta)\right]_{A'}^{B'}, \tag{10}$$

and the continuity conditions, Eqs. (4) and (5), become

$$w_1 = w_2,\ T_1 = T_2 \text{ on } \mathbf{\Pi}_1, \tag{11}$$

$$T_2 = 0 \text{ on } \mathbf{\Pi}_2. \tag{12}$$

The substitution of Eqs. (7) into (6) yields

$$\varphi_2(\zeta) = \varphi_{2S}(\zeta) + \varphi_{20}(\zeta) \text{ in } D_2', \tag{13}$$

where the constant term representing the rigid displacement is neglected, the singular part

$$\varphi_{2S}(\zeta) = \frac{\mu_2 b}{2\pi\mathrm{i}} \ln\frac{\zeta - \zeta_0}{\zeta + R_2}, \tag{14}$$

and the holomorphic function $\varphi_{20}(\zeta)$ can be expanded into a Laurent series in the annular region D_2'

$$\varphi_{20}(\zeta) = G_P(\zeta) + G_N(\zeta) = \sum_{n=1}^{\infty} C_n \zeta^n + \sum_{n=1}^{\infty} D_n \zeta^{-n} \text{ for } R_1 < |\zeta| < R_2. \tag{15}$$

In Eq. (15),$G_P(\zeta)$ and $G_N(\zeta)$ represent the sums of the positive and negative power terms with the undetermined complex constants C_n and D_n, respectively.

3.2 Analytic continuation and solution

For the convenience of analysis, the following new analytical functions are introduced in the corresponding regions according to the Schwarz symmetry principle.

$$\varphi_{1*}(\zeta) = -\overline{\varphi_1}\left(R_1^2/\zeta\right) \text{ for } |\zeta| > R_1, \tag{16}$$

$$\varphi_{2*}(\zeta) = -\overline{\varphi_2}\left(R_1^2/\zeta\right) = \frac{\mu_2 b}{2\pi\mathrm{i}} \ln\frac{\zeta - R_1^2/\overline{\zeta_0}}{\zeta + R_1^2/R_2} + \varphi_{2*0}(\zeta) \text{ for } R_1^2/R_2 < |\zeta| < R_1, \tag{17}$$

$$\varphi_{2**}(\zeta) = -\overline{\varphi_2}\left(R_2^2/\zeta\right) = \frac{\mu_2 b}{2\pi\mathrm{i}} \ln\frac{\zeta - R_2^2/\overline{\zeta_0}}{\zeta + R_2} + \varphi_{2**0}(\zeta) \text{ for } R_2 < |\zeta| < R_2^2/R_1, \tag{18}$$

where $\varphi_{2*0}(\zeta) = -\overline{G_P}\left(R_1^2/\zeta\right) - \overline{G_N}\left(R_1^2/\zeta\right)$, $\varphi_{2**0}(\zeta) = -\overline{G_P}\left(R_2^2/\zeta\right) - \overline{G_N}\left(R_2^2/\zeta\right)$. With the aid of these functions and basic equations, the continuity conditions of displacements and stresses, Eqs. (11) and (12), can be reduced to the following functional equations

$$[\mu_2\varphi_1(t) + \mu_1\varphi_{2*}(t)]_{D_1'} = [\mu_2\varphi_{1*}(t) + \mu_1\varphi_2(t)]_{D_2'} \text{ on } \mathbf{\Pi}_1, \tag{19}$$

$$\begin{cases} [\varphi_{2*}(t) - \varphi_1(t)]_{D_1'} = [\varphi_{1*}(t) - \varphi_2(t)]_{D_2'} \text{ on } \mathbf{\Pi}_1 \\ [\varphi_{1*}(t) - \varphi_2(t)]_{D_2'} = [\varphi_{1*}(t) + \varphi_{2**}(t)]_{D_3'} \text{ on } \mathbf{\Pi}_2 \end{cases}, \tag{20}$$

where the subscripts D_1, D_2 and D_3 refer to the function values as approached from the three corresponding regions, respectively.

By using the sectionally holomorphic function theory [18] and the Cauchy integral technique, an exact series solution for the problem is obtained

$$\varphi_1(\zeta) = -\overline{G_N}\left(R_1^2/\zeta\right) + \frac{\mu_2 b}{2\pi \mathrm{i}} \ln \frac{\zeta - \zeta_0}{\zeta + R_2} + \frac{\mu_2 b}{2\pi \mathrm{i}} \ln \frac{\zeta + R_2}{\zeta - R_2^2/\overline{\zeta_0}} - \overline{G_N}\left(R_2^2/\zeta\right), \tag{21}$$

$$\begin{aligned}\varphi_2(\zeta) = {} & \frac{\mu_2 b}{2\pi \mathrm{i}} \ln \frac{\zeta - \zeta_0}{\zeta + R_2} - k\overline{G_P}\left(R_1^2/\zeta\right) + \frac{1-k}{2}\overline{G_N}\left(R_2^2/\zeta\right) + \frac{1+k}{2} G_P(\zeta) \\ & + \frac{k\mu_2 b}{2\pi \mathrm{i}} \ln \frac{\zeta - R_1^2/\overline{\zeta_0}}{\zeta + R_1^2/R_2} + \frac{(1-k)\mu_2 b}{4\pi \mathrm{i}} \ln \frac{\zeta + R_2}{\zeta - R_2^2/\overline{\zeta_0}},\end{aligned} \tag{22}$$

where the parameter

$$k = \frac{\mu_1 - \mu_2}{\mu_1 + \mu_2}, \tag{23}$$

where μ_1 and μ_2 are the shear modulus of the inhomogeneity and matrix, respectively. The remaining work is to determine the coefficients C_n and D_n in Eq. (15). Noting that

$$\ln \frac{\zeta - R_1^2/\overline{\zeta_0}}{\zeta + R_1^2/R_2} = \sum_{n=1}^{\infty} \frac{(-1)^n R_1^{2n} R_2^{-n} - R_1^{2n}\overline{\zeta_0}^{-n}}{n} \cdot \zeta^{-n},$$

$$\ln \frac{\zeta - R_2^2/\overline{\zeta_0}}{\zeta + R_2} = \sum_{n=1}^{\infty} \frac{(-1)^n R_2^{-n} - R_2^{-2n}\overline{\zeta_0}^{n}}{n} \cdot \zeta^{n},$$

and substituting them into Eq. (22), a comparison of the coefficients of the same power terms in Eqs. (13) and (22) yields the complex coefficients

$$\begin{cases} C_n = -\frac{\mu_2 b}{2\pi \mathrm{i}} \frac{(-1)^n R_2^{-n}}{n} + \frac{\mu_2 b}{2\pi \mathrm{i}} \frac{\overline{\zeta_0}^{n} R_2^{-2n} + k\zeta_0^{-n} R_1^{2n} R_2^{-2n}}{n\left(1 + kR_1^{2n} R_2^{-2n}\right)} \\ D_n = \frac{\mu_2 b}{2\pi \mathrm{i}} \frac{k\left(\zeta_0^{n} R_1^{2n} R_2^{-2n} - \overline{\zeta_0}^{-n} R_1^{2n}\right)}{n\left(1 + kR_1^{2n} R_2^{-2n}\right)} \end{cases}. \tag{24}$$

The substitution of Eq. (24) into (22) and transforming to the z-plane yield

$$\begin{aligned} f_2(z) = {} & \frac{\mu_2 b}{2\pi \mathrm{i}} \ln(z - z_0) + \frac{k\mu_2 b}{2\pi \mathrm{i}} \ln \frac{z - R_1^2/\overline{z_0}}{z - R_1^2/R_2} - \frac{(1-k)\mu_2 b}{4\pi \mathrm{i}} \ln(z + \overline{z_0} - 2(R_1 + h)) \\ & + \frac{k\mu_2 b}{2\pi \mathrm{i}} \sum_{n=1}^{\infty} \frac{\mathrm{A}^n + k\overline{\mathrm{A}}^{-n} R_1^{-2n}}{n(\beta^{-2n} + k)} \cdot \left(\frac{z + a}{az + R_1^2}\right)^{-n} - \frac{(1+k)\mu_2 b}{4\pi \mathrm{i}} \ln(z - R_2) \\ & + \frac{\mu_2 b}{2\pi \mathrm{i}} \sum_{n=1}^{\infty} \frac{(1 + k - k\beta^{2n} + k^2\beta^{2n})\overline{\mathrm{A}}^{n} R_1^{2n} + 2k\mathrm{A}^{-n}}{2n(\beta^{-2n} + k)} \cdot \left(\frac{z + a}{az + R_1^2}\right)^{n} \end{aligned} \tag{25}$$

where $\mathrm{A} = \frac{z_0 + a}{az_0 + R_1^2}$, $\beta = R_1/R_2$.

4 A discussion on the complex potential solution

In this section, special cases of the solution of the complex potential are examined, not only to check correction of the present solution, but also to seek a new expression of the solution, which is of physical significance (various interaction effects are separated) and of mathematical elegance (much better convergence). In the following, we discuss only the special cases of $f_2(z)$ in Eq. (25), which determines the internal force acting on the dislocation.

4.1 Special cases

4.1.1 A screw dislocation in an infinite medium

Letting $\mu_1 = \mu_2$ and $h \to \infty$ (i.e., $k = 0$ and $R_2 \to \infty$), Eq. (25) degenerates into the solution of a screw dislocation in an infinite medium

$$f_{\text{Inf}}(z) = \frac{\mu_2 b}{2\pi \mathrm{i}} \ln(z - z_0), \tag{26}$$

which is in agreement with the previous result from Muskhelishvili [18].

4.1.2 A screw dislocation near the free surface in a semi-infinite medium

Letting $\mu_1 = \mu_2$, Eq. (25) degenerates to the solution of a screw dislocation near the free surface in a semi-infinite medium

$$f_{\text{Surf}}(z) = f_{\text{Inf}}(z) + f_{\text{Surf0}}(z), \tag{27}$$

where $f_{\text{Inf}}(z)$ is given in Eq. (26) and $f_{\text{Surf0}}(z)$ is a holomorphic function in the matrix region, which reflects the interaction of the screw dislocation with the free surface

$$f_{\text{Sur0}}(z) = -\frac{\mu_2 b}{2\pi \mathrm{i}} \ln\left(z + \overline{z_0} - 2(R_1 + h)\right). \tag{28}$$

By a simple coordinate transformation, Eq. (27) reverts to the previous solution given by Head [1].

4.1.3 A screw dislocation near a circular inhomogeneity in an infinite medium

Letting $h \to \infty$, Eq. (25) degenerates to the solution of a screw dislocation near a circular inhomogeneity in an infinite medium.

$$f_{\text{Inh}}(z) = f_{\text{Inf}}(z) + f_{\text{Inh0}}(z), \tag{29}$$

where $f_{\text{Inh0}}(z)$ is a holomorphic function in the matrix region, which reflects the interaction of the screw dislocation with the circular inhomogeneity

$$f_{\text{Inh0}}(z) = \frac{k\mu_2 b}{2\pi \mathrm{i}} \ln \frac{z - R_1^2/\overline{z_0}}{z}. \tag{30}$$

Eq. (29) is in agreement with the previous solution from Smith's work [2].

4.2 Complex potential with various interaction effects separated

Section 4.1 gives us a significant hint that the complex potential $f_2(z)$ can be cast into a new expression $f_{2\text{New}}(z)$, where various interaction effects are separated:

$$f_{2\text{New}}(z) = f_{\text{Inf}}(z) + f_{\text{Surf0}}(z) + f_{\text{Inh0}}(z) + f_{\text{Cpl}}(z), \tag{31}$$

where $f_{\text{Inf}}(z)$, $f_{\text{Surf0}}(z)$ and $f_{\text{Inh0}}(z)$ refer to Eqs. (26), (28), and (30), respectively. $f_{\text{Surf0}}(z)$ and $f_{\text{Inh0}}(z)$ reflect the interactions of the screw with the free surface and circular inhomogeneity, respectively. Compared with Eq. (25), the residual part $f_{\text{Cpl}}(z)$ can be written as

$$\begin{aligned} f_{\text{Cpl}}(z) = &- \ln\left(\frac{z - R_1^2/R_2}{z}\right) + \frac{k\mu_2 b}{2\pi \mathrm{i}} \sum_{n=1}^{\infty} \frac{\mathrm{A}^n + k\overline{\mathrm{A}}^{-n} R_1^{-2n}}{n(\beta^{-2n} + k)} \cdot \left(\frac{z + a}{az + 1}\right)^{-n} \\ &+ \frac{k\mu_2 b}{2\pi \mathrm{i}} \sum_{n=1}^{\infty} \frac{\mathrm{A}^{-n} - \overline{\mathrm{A}}^{n} R_1^{2n} \beta^{2n}}{n(\beta^{-2n} + k)} \cdot \left(\frac{z + a}{az + 1}\right)^{n}, \end{aligned} \tag{32}$$

which reflects a coupling interaction caused by the free surface and the circular inhomogeneity. From its physical meaning, $f_{\text{Cpl}}(z)$ represents a higher-order interaction effect than $f_{\text{Surf0}}(z)$ and $f_{\text{Inh0}}(z)$, so Eq. (31) more rapidly converges than Eq. (25), which will be further discussed in Sect. 5.2.

5 Interaction energy and image force

5.1 Fundamental theory and nondimensional expressions

The interaction energy and image force acting on dislocation are of practical importance in understanding the behavior of inhomogeneous materials. The strain energy due to the presence of a dislocation is equal to the work required to introduce the dislocation into the material. The displacement along the dislocation is just the module b of the Burgers vector $\boldsymbol{b}$, and the total force on the dislocation can be calculated from Eq. (3). Thus, the strain energy W is given by [19]

$$W = \frac{1}{2} bT, \tag{33}$$

where T refers to Eq. (3).The interaction energy is the difference between W and the self-energy of the screw dislocation in the homogeneous material, which can be formally written as

$$\Delta W = \frac{1}{2} b \mathrm{Im} \left[\Delta f_2(z_0) \right], \tag{34}$$

where Im denotes the imaginary part of a complex quantity, and Δ represents the part of the complex potential after removing the dislocation singularity. By substituting Eqs. (25) or (31) into (34) and dividing both sides by $\mu_2 b^2/(4\pi)$, the nondimensional interaction energy can be written as

$$\tilde{W} = \frac{4\pi}{\mu_2 b^2} \Delta W = \frac{2\pi}{\mu_2 b} \mathrm{Im} \left[f_{20}(z_0) \right]. \tag{35}$$

According to the Peach–Koehler formula, the image force at the point z_0 is [20]

$$F_x - \mathrm{i} F_y = \mathrm{i} b \left[\hat{\tau}_{xz2}(z_0) - \mathrm{i} \hat{\tau}_{yz2}(z_0) \right], \tag{36}$$

where F_x and F_y are the force components in the x-axis and y-axis directions, respectively. $\hat{\tau}_{xz2}(z_0)$ and $\hat{\tau}_{yz2}(z_0)$ denote the perturbation stress components at the dislocation point, which can be derived by subtracting those attributions to the dislocation in the corresponding infinite homogeneous medium from the obtained stresses, then taking the limit as z approaches z_0. The substitution of Eqs. (2) and (25) [or (31)] into (36) and dividing both sides by $\mu_2 b^2/(2\pi R_1)$ yield the nondimensional image force

$$\tilde{F} = \frac{2\pi R_1}{\mu_2 b^2} \left(F_x - \mathrm{i} F_y \right) = \frac{2\pi R_1 \mathrm{i}}{\mu_2 b} \left[f'_{20}(z) \right]_{z=z_0}. \tag{37}$$

The nondimensional physical quantities, $\tilde{W}$ and $\tilde{F}$, both are functions of the position coordinates of the dislocation.

5.2 Convergence of the nondimensional image force

In this subsection, numerical examples are presented to compare the convergence of the two expressions (25) and (31) of the complex potential solution.

Computations show that the interaction energy varies most rapidly on H_1H_2 of the x-axis (Fig. 1a). From Eq. (37), $F_y = 0$ in the x-axis and $\tilde{F} = 2\pi R_1 F_x/\mu_2 b^2$.

Without loss of generality, we introduce a relative location of dislocation

$$\delta = \frac{x - R_1}{h}, \tag{38}$$

where h is the length of H_1H_2 in Fig. 1a. Take five representative points on H_1H_2 : $\delta = 0.01, 0.25, 0.5, 0.75, 0.99$. Without loss of generality, define a nondimensional distance $\tilde{h} = h/R_1$. Consider four typical properties of the inhomogeneity: (1) a hole ($k = -1$), (2) a soft inhomogeneity ($k = -0.5$), (3) a hard inhomogeneity ($k = 0.5$), and (4) a rigid inhomogeneity ($k = 1$). By using $f_{2\mathrm{New}}(z)$ in Eq. (31) and $f_2(z)$ in Eq. (25), the number N_0 of terms in series required at a 1 % truncation error of the nondimensional image force $\tilde{F} = 2\pi R_1 F_x/\mu_2 b^2$ is listed in Table 1.

Table 1 The number N_0 of terms in series required at a 1 % truncation error of the nondimensional image force $\tilde{F} = 2\pi R_1 F_x/\mu_2 b^2$ for 5 values of the relative location $\delta = (x - R_1)/h$ and 4 values of the material parameter k, where the nondimensional distance $\tilde{h} = h/R_1 = 1$

$k = \frac{\mu_1-\mu_2}{\mu_1+\mu_2}$	Number of terms N_0									
	$\delta = 0.01$		$\delta = 0.25$		$\delta = 0.50$		$\delta = 0.75$		$\delta = 0.99$	
	$f_{2\text{New}}$	f_2	$f_{2\text{New}}$	f_2	$f_{2\text{New}}$	f_2	$f_{2\text{New}}$	f_2	$f_{2\text{New}}$	f_2
−1	0	0	2	2	1	1	1	1	0	0
−0.5	0	0	1	3	1	3	1	6	0	139
0.5	0	0	1	2	1	3	1	7	0	187
1	0	0	1	2	1	4	1	8	0	199

Table 2 The number N_0 of terms in series required at a 1 % truncation error of the nondimensional image force $\tilde{F} = 2\pi R_1 F_x/\mu_2 b^2$ for 5 values of the nondimensional distance $\tilde{h} = h/R_1$ and 4 values of the material parameter k, where the relative location $\delta = (x - R_1)/h = 0.75$

$k = \frac{\mu_1-\mu_2}{\mu_1+\mu_2}$	Number of terms N_0									
	$\tilde{h} = 10$		$\tilde{h} = 5$		$\tilde{h} = 1$		$\tilde{h} = 0.5$		$\tilde{h} = 0.05$	
	$f_{2\text{New}}$	f_2	$f_{2\text{New}}$	f_2	$f_{2\text{New}}$	f_2	$f_{2\text{New}}$	f_2	$f_{2\text{New}}$	f_2
−1	0	0	0	0	1	1	1	1	4	4
−0.5	0	3	0	4	1	6	1	7	3	21
0.5	0	5	0	5	1	7	1	10	3	27
1	0	5	0	5	1	8	1	10	4	29

It is seen from Table 1 that $f_{2\text{New}}(z)$ converges more rapidly than $f_2(z)$. In most cases, only one term ($N_0 = 1$) is needed to ensure that the error is $< 1\,\%$. It is noticed that for a hole, the point $\delta = 0.25$ is very close to the equilibrium point where the image force is equal to zero (refer to Fig. 5).

The influence of the nondimensional distance $\tilde{h}$ on the number N_0 of terms in series is shown in Table 2 at a 1 % truncation error. It is seen from Table 2 that with the decrease of $\tilde{h}$, N_0 rapidly increases for $f_2(z)$, whereas except for a very small distance, only one term is needed with $f_{2\text{New}}(z)$. Even if the value of $\tilde{h}$ is very small, N_0 required with $f_{2\text{New}}(z)$ is much smaller than that with $f_2(z)$.

5.3 Simple approximate solution

From Sect. 5.2, it is seen that attributing to uncoupling of various interaction effects, in most cases the first-order approximation $f_{2\text{App}}(z)$ of the complex potential solution $f_{2\text{New}}(z)$ in Eq. (31),

$$f_{2\text{App}}(z) = \frac{\mu_2 b}{2\pi \mathrm{i}} \ln(z - z_0) + \frac{k\mu_2 b}{2\pi \mathrm{i}} \ln \frac{z - R_1^2/\overline{z_0}}{z - R_1^2/R_2} - \frac{\mu_2 b}{2\pi \mathrm{i}} \ln(z + \overline{z_0} - 2(R_1 + h)) + \frac{k\mu_2 b}{2\pi \mathrm{i}} \frac{\mathrm{A}^{-1} - \overline{\mathrm{A}} R_1^2 \beta^2}{\beta^{-2} + k} \frac{z + a}{az + 1} + \frac{k\mu_2 b}{2\pi \mathrm{i}} \frac{\mathrm{A} + k\overline{\mathrm{A}}^{-1} R_1^{-2}}{\beta^{-2} + k} \frac{az + 1}{z + a}, \tag{39}$$

has high accuracy. In order to demonstrate the accuracy of the simple approximate solution (39), the curves of the nondimensional image force $\tilde{F} = 2\pi R_1 F_x/\mu_2 b^2$ versus the relative location δ are depicted in Fig. 2 for a hard and rigid inhomogeneity and in Fig. 3 for a soft inhomogeneity and a hole, respectively. From Figs. 2 and 3, it is seen that the accuracy of the simple approximate solution is so high that it cannot be distinguished from the exact solution. Of course, as seen from Table 2, for a very small value of $\tilde{h}$, the higher-order solution is still required.

5.4 Distribution of the interaction energy and image force

In the previous sections, the full-field solution of the complex potential is derived, in terms of which the interaction energy and the image force of a screw dislocation can be evaluated.

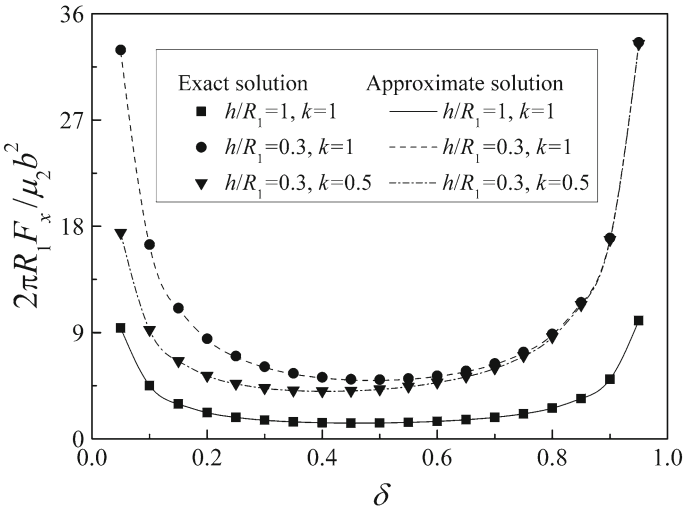

Fig. 2 Nondimensional image force $\tilde{F} = 2\pi R_1 F_x/\mu_2 b^2$ versus the relative location δ by using the exact and approximate solutions for rigid ($k = 1$) and hard ($k = 0.5$) inhomogeneities, where $\delta = (x - R_1)/h$, $k = (\mu_1 - \mu_2)/(\mu_1 + \mu_2)$

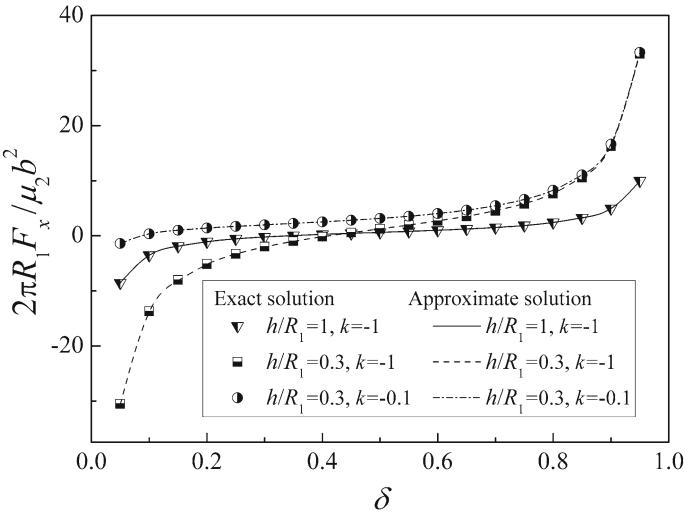

Fig. 3 Nondimensional image force $\tilde{F} = 2\pi R_1 F_x/\mu_2 b^2$ versus the relative location δ by using the exact and approximate solutions for a hole ($k = -1$) and soft ($k = -0.5$) inhomogeneity, where $\delta = (x - R_1)/h$, $k = (\mu_1 - \mu_2)/(\mu_1 + \mu_2)$

Consider a circular hard inhomogeneity ($k = 0.5$), and let the nondimensional distance between the inhomogeneity and free surface $\tilde{h} = h/R_1 = 1$. The distribution of the nondimensional interaction energy $\tilde{W}$ and image force $\tilde{F}$ is depicted in Fig. 4, where $\tilde{W}$ and $\tilde{F}$ refer to Eqs. (35) and (37), respectively. It is seen that the coupling interaction effects induced by the inhomogeneity and free surface severely distort the interaction energy contour (dashed lines where the values of $\tilde{W}$ are marked) and image force line (solid lines where the directions of $\tilde{F}$ are marked). As predicted, the two families of curves still keep being orthogonal to each other. The image force lines first leave along the outer normal of the inhomogeneity, and then gradually turn to the free surface. The interaction energy contour lines vary most dramatically on the interval (1, 2) of the x-axis. With the increase in the distance from the inhomogeneity, the interaction effect induced by the inhomogeneity decays. An unstable equilibrium point of the screw dislocation is found at the point $E(\tilde{x} = x/R_1 = -1.87)$.

The interaction energy contour and image force line induced by the interaction of a screw dislocation with a circular hole ($k = -1$) near the free surface are depicted in Fig. 5, where $\tilde{h} = 1$. An unstable equilibrium point is found at the point E ($\tilde{x} = x/R_1 = 1.34$).

When the inhomogeneity is far from the free surface, the diagram approaches to the case that there is no free surface. The diagram is not depicted to save space.

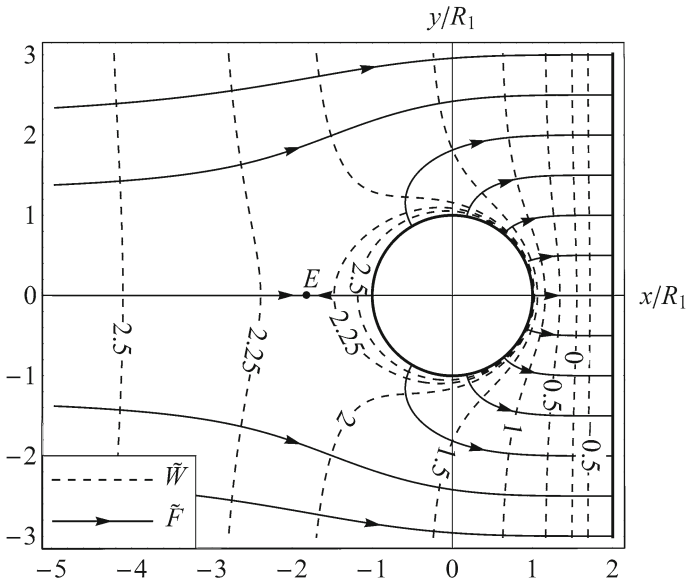

Fig. 4 The nondimensional interaction energy contour (*dashed lines* where the values of $\tilde{W}$ are *marked*) and image force line (*solid lines* where the directions of $\tilde{F}$ are *marked*) induced by the interaction of a screw dislocation with a circular hard inhomogeneity ($k = (\mu_1 - \mu_2)/(\mu_1 + \mu_2) = 0.5$) near the free surface, where the nondimensional distance between the inhomogeneity and free surface $\tilde{h} = h/R_1 = 1$

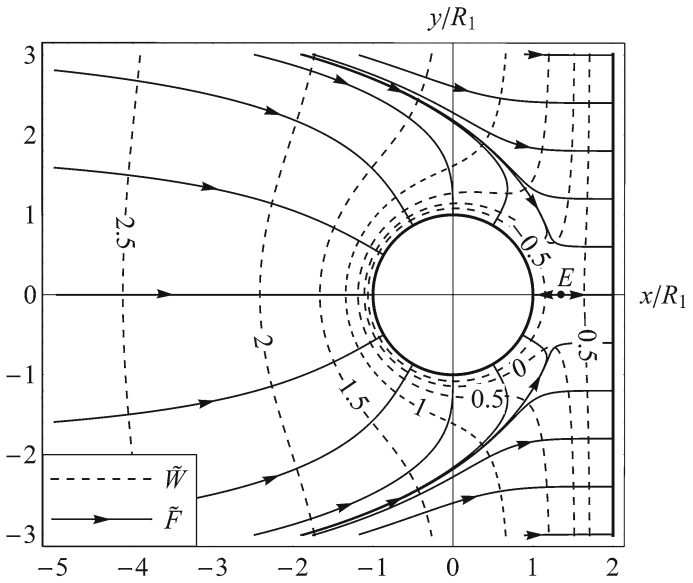

Fig. 5 The nondimensional interaction energy contour (*dashed lines* where the values of $\tilde{W}$ are *marked*) and image force line (*solid lines* where the directions of $\tilde{F}$ are *marked*) induced by the interaction of a screw dislocation with a circular hole ($k = (\mu_1 - \mu_2)/(\mu_1 + \mu_2) = -1$) near the free surface, where the nondimensional distance between the inhomogeneity and free surface $\tilde{h} = h/R_1 = 1$

6 Conclusion

(1) The interaction of a screw dislocation with a circular inhomogeneity near the free surface is dealt with. By using the complex potential and conformal mapping technique, an explicit series solution is obtained and many existing solutions can be reobtained as the special cases of the present solution.
(2) The present solution is cast into a new expression where various interaction effects are separated. The new expression converges more rapidly, and a simple approximate formula with high accuracy is presented.

(3) The full-field interaction energy and image force are evaluated and shown graphically. It is found that in the case of a soft inhomogeneity or hole, there is an unstable equilibrium point of the screw dislocation between the inhomogeneity and free surface, whereas in the case of a hard or rigid inhomogeneity, there is a unstable equilibrium point on the opposite side of the inhomogeneity. When the screw dislocation, inhomogeneity, and free surface are close to each other, the interaction energy and image force exhibit a strong and intricate coupling in the near field.

The present work has led to a much improved understanding of coupling interaction among the dislocation, inhomogeneity, and free surface.

Acknowledgments The work was supported by the National Natural Science Foundation of China (Grant Nos. 11172023, 11061130550 and 91216110).

References

1. Head, A.K.: The interaction of dislocations and boundaries. Philos. Mag. **44**, 92–94 (1953)
2. Smith, E.: The interaction between dislocations and inhomogeneities-I. Int. J. Eng. Sci. **6**, 129–143 (1968)
3. Li, Z.H., Shi, J.Y.: The interaction of a screw dislocation with inclusion analyzed by Eshelby equivalent inclusion method. Scripta Mater. **47**, 371–375 (2002)
4. Shen, M.H., Chen, S.N., Lin, C.P.: The interaction between a screw dislocation and a piezoelectric fiber composite with a wedge crack. Arch. Appl. Mech. **82**, 215–227 (2012)
5. Zeng, X., Fang, Q.H., Liu, Y.W.: Exact solutions for piezoelectric screw dislocations near two asymmetrical edge cracks emanating from an elliptical hole. Arch. Appl. Mech. **83**, 1097–1107 (2013)
6. Zhang, J., Qu, Z., Huang, Q.Q., Xie, L.C., Xiong, C.B.: Interaction between cracks and a circular inclusion in a finite plate with the distributed dislocation method. Arch. Appl. Mech. **83**, 861–873 (2013)
7. Xiao, Z.M., Chen, B.J.: A screw dislocation interacting with a coated fiber. Mech. Mater. **32**, 485–494 (2000)
8. Jiang, C.P., Xu, Y.L., Liu, Y.W.: Interaction of a screw dislocation in the interphase layer with the inclusion and matrix. Appl. Math. Mech. **24**, 979–988 (2003)
9. Honein, E., Rai, H., Najjar, M.I.: The material force acting on a screw dislocation in the presence of a multi-layered circular inclusion. Int. J. Solids Struct. **43**, 2422–2440 (2006)
10. Sudak, L.J.: On the interaction between a dislocation and a circular inhomogeneity with imperfect interface in antiplane shear. Mech. Res. Commun. **30**, 53–59 (2003)
11. Fang, Q.H., Liu, Y.W.: Size-dependent elastic interaction of a screw dislocation with a circular nano-inhomogeneity incorporating interface stress. Scripta Mater. **55**, 99–102 (2006)
12. Luo, J., Xiao, Z.M.: Analysis of a screw dislocation interacting with an elliptical nano inhomogeneity. Int. J. Eng. Sci. **47**, 883–892 (2009)
13. Ahmadzadeh-Bakhshayesh, H., Gutkin, M.Yu., Shodja, H.M.: Surface/interface effects on elastic behavior of a screw dislocation in an eccentric core-shell nanowire. Int. J. Solids Struct. **49**, 2422–2440 (2012)
14. Gilman, J.J., Johnston, W.G.: Observations of dislocation glide and climb in lithium fluoride crystals. J. Appl. Phys. **27**, 1018–1022 (1956)
15. D'Aragona, F.S.: Dislocation etch for (100) planes in silicon. J. Electrochem. Soc. **119**, 948–951 (1972)
16. Osakabe, N., Endo, J., Matsuda, T., Tonomura, A., Fukuhara, A.: Observation of surface undulation due to single-atomic shear of a dislocation by reflection-electron holography. Phys. Rev. Lett. **62**, 2969–2972 (1989)
17. Fuente, O.R., Zimmerman, J.A., González, M.A., Figuera, J., Hamilton, J.C., Pai, W.W., Rojo, J.M.: Dislocation emission around nanoindentations on a (001) fcc metal surface studied by scanning tunneling microscopy and atomistic simulations. Phys. Rev. Lett. **88**, 036101 (2002)
18. Muskhelishvili, N.I.: Some Basic Problems of the Mathematical Theory of Elasticity. Noorhoff, Groningen, Holland (1953)
19. Gong, S.X., Meguid, S.A.: A screw dislocation interacting with an elastic elliptical inhomogeneity. Int. J. Eng. Sci. **32**, 1221–1228 (1994)
20. Shi, J., Li, Z.: An approximate solution of the interaction between an edge dislocation and an inclusion of arbitrary shape. Mech. Res. Commun. **33**, 804–810 (2006)